remote sensing

MDPI

Article

The Evolution of Powell Basin (Antarctica)

Alberto Santamaría Barragán [1,*], Manuel Catalán [2,†] and Yasmina M. Martos [3,4,5]

[1] Chemistry Science Building, University of Salamanca, 37008 Salamanca, Spain
[2] Formerly at the Department of Geophysics, Royal Observatory of the Spanish Navy, 11100 San Fernando, Spain
[3] Planetary Magnetospheres Laboratory, NASA Goddard Space Flight Center, Greenbelt, MD 20771, USA; yasmina.martos@nasa.gov
[4] Department of Astronomy, University of Maryland, College Park, MD 20742, USA
[5] Center for Research and Exploration in Space Science &Technology II, Greenbelt, MD 20771, USA
* Correspondence: betobaltanas@usal.es
† Deceased.

Abstract: Powell Basin is an ocean basin formed as a result of the Scotia Sea evolution. The existing tectonic models propose a variety of starting and ending ages for the spreading of the basin based on seafloor magnetic anomalies. Here, we use recent magnetic field data obtained from eight magnetic profiles in Powell Basin to provide insights into the oceanic spreading evolution. The differences found between the number of anomalies on both sides of the axis and the asymmetry in the spreading rates suggest different opening models for different parts of the basin. We propose a spreading model starting in the late Eocene (38.08 Ma) and ending in the early Miocene (21.8 Ma) for the northern part of Powell Basin. For the southern part, the opening started in the late Eocene (38.08 Ma) and ended in the middle Paleogene (25.2 Ma). The magnetic data have been combined with gravity and sediment thickness data to better constrain the age models. The gravity and sediment thickness information allow us to more accurately locate the position of the extinct spreading axis. Geothermal heat flow measurements are used to understand the relationship between the low amplitudes of the magnetic anomalies and the heat beneath them. Our proposed oceanic spreading models suggest that the initial incursions of the Pacific mantle outflow into the Powell Basin occurred in the Oligocene, and the initial incursions of oceanic currents from the Weddell Sea occurred in the Eocene.

Keywords: magnetic anomalies; oceanic spreading; asthenospheric currents; oceanic currents

Citation: Santamaría Barragán, A.; Catalán, M.; Martos, Y.M. The Evolution of Powell Basin (Antarctica). *Remote Sens.* **2024**, *16*, 4053. https://doi.org/10.3390/rs16214053

Academic Editors: Manuel Berrocoso Domínguez, Gonçalo Prates and Cristina Torrecillas

Received: 12 September 2024
Revised: 20 October 2024
Accepted: 24 October 2024
Published: 31 October 2024

1. Introduction

Continental drifting is a major geological process that involves the movement and evolution of continental land masses [1]. There are several geological and geophysical methods (e.g., magnetic anomalies, paleontology, paleomagnetism, and structural geology) that are frequently used by the community to provide information on the understanding of continental drifting processes. The study of magnetic anomalies is one of the most widely used methods to study these processes since it provides constraints for understanding the geodynamic history and evolution of a region [2,3].

Great examples of plate tectonics and oceanic spreading are found in the Scotia Sea and surrounding areas as a consequence of the separation of the South American plate from the Antarctic plate [4,5]. For example, the Dove, Ona and Protector Basins are in the southern part of the Scotia Sea, and the Powell Basin is located to the northeast of the Antarctic Peninsula (Figure 1). The study of these basins through various geophysical and geological data and techniques provides information and constraints about the geodynamic evolution of this region as well as the continental break up of South America and Antarctica.

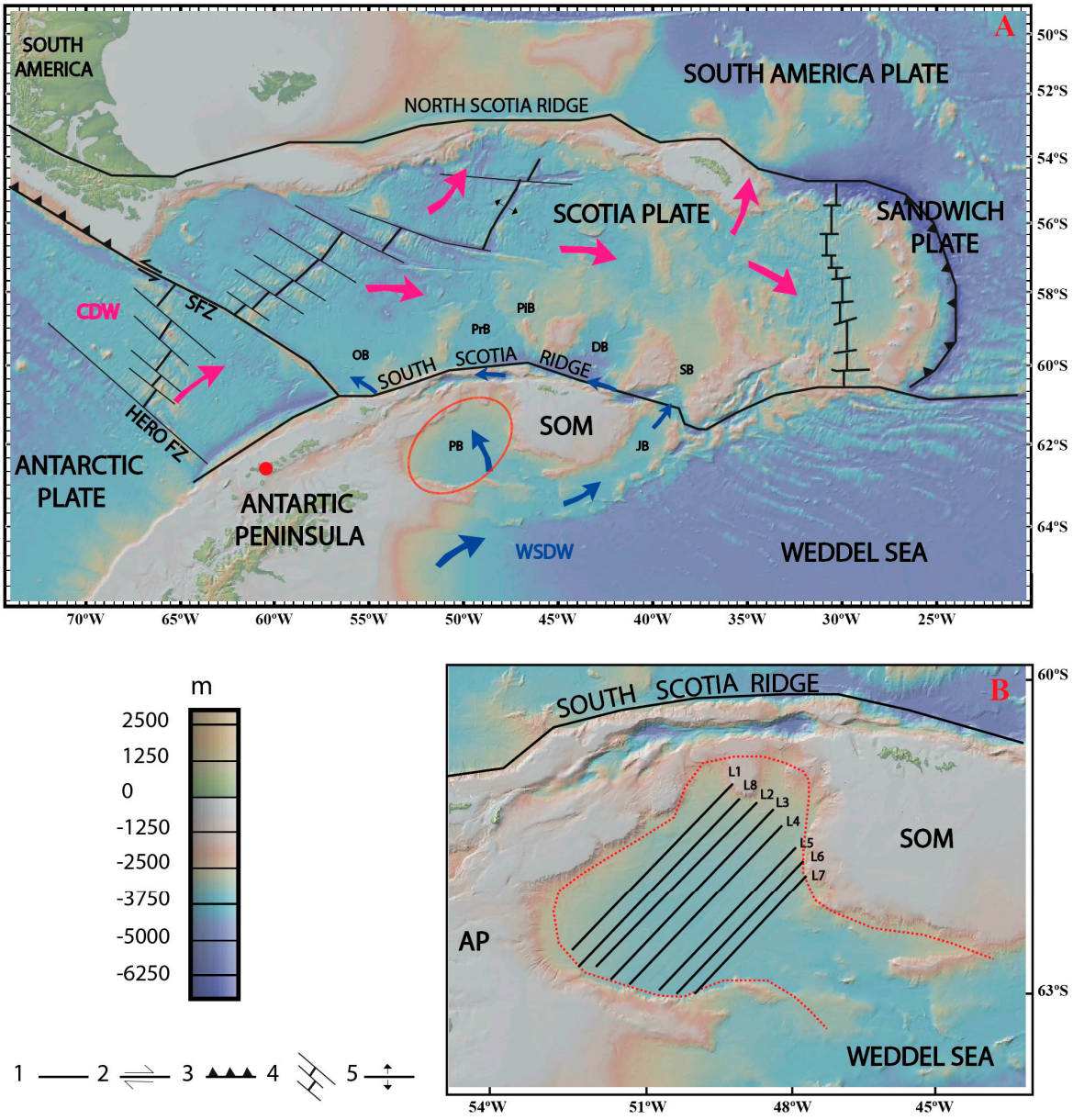

Figure 1. Scotia Sea and Powell Basin setting. (**A**) Bathymetry and geological setting of the study area (modified from Global Multi-Resolution Topography data grid GMRT [6]). The red dot indicates the geographical position of the magnetic observatory in Livingston Island. (**B**) Bathymetry map of the Powell Basin with magnetic profiles obtained during the ElGeoPoweR expedition. Morphological and oceanographic features: AP, Antarctic Peninsula; DB, Dove Basin; JB, Jane Basin; OB, Ona Basin; PB, Powell Basin; Pib, Pirie Basin; PrB, Protector Basin; SB, Scan Basin; SFZ, Shackleton Fracture Zone; SOM, South Orkney Microcontinent; 1, Active fracture zone; 2, Transcurrent fault; 3, Active subduction zone; 4, Active spreading center; and 5, Active extensional zone. Water masses: CDW, Circumpolar Deep Water; WSDW, Weddell Sea Deep Water.

Seafloor spreading models derived by studying oceanic magnetic anomalies are, in occasions, subject of debate, proposing different ages for the opening and evolution of basins and providing different views of geodynamic evolution characteristics [7–10]. Also, other kinds of crustal magnetic anomalies provide insights into continental break-up, subduction, or other geodynamic processes. In the case of the Antarctic Peninsula and surrounding areas, magnetic data have allowed the identification of the Pacific Margin Anomaly (PMA), which is a batholitic complex with a high amplitude magnetic anomaly

signature that can be observed in places like the South Shetland Islands and the South Orkney Microcontinent [11–13].

The geodynamic evolution of the Powell Basin as well as its geographic location (Figure 1) is of great interest as it provides information on (1) the break-up history of the South Orkney Microcontinent (SOM) from the Antarctic Peninsula [13–15], (2) the evolution of oceanic currents between the Weddell Sea and Scotia Sea [16,17], and (3) the presence of asthenospheric flows [18–21].

The multidisciplinary Antarctic expedition "ElGeoPoweR" was carried out in January 2022. During this survey, new geothermal heat flow and magnetic field measurements were collected in Powell Basin, including eight magnetic profiles perpendicular to the spreading axis (Figure 1B). The objectives of our study are to propose an updated oceanic spreading model that sheds light on the geodynamic evolution of the Powell Basin and the continental drift of the SOM and to evaluate their regional consequences on oceanic and asthenospheric currents.

2. Geological Setting

During the Oligocene, the Drake Passage opened as a consequence of the separation of South America and the Antarctic Peninsula. The tectonic events led to the separation of continental blocks forming the Scotia Sea [6,13,22–26]. A series of small oceanic basins (e.g., Protector Basin, Dove Basin, Ona Basin, Scan Basin, and Powell Basin) (Figure 1) formed in the southern part of the Scotia Sea and in the Weddell Sea as a result of the tectonic extension [27–30].

Our study area, Powell Basin, is bounded by three continental boundaries and one oceanic boundary. The continental boundaries are the Antarctic Peninsula to the west (AP), the SOM to the east, and the South Scotia Ridge (SSR) to the north. The oceanic boundary is the Weddell Sea to the south (Figure 1) [14,31].

Tectonically, the evolution of the Powell Basin remains under discussion. The existence of low-amplitude magnetic anomalies throughout the basin has been the subject of controversy for years. These low amplitudes are the reason why assigning accurate ages for the opening and evolution of the basin by using oceanic spreading magnetic anomalies is so complex [7,14,20,32,33].

Some authors [14] propose an evolutionary model of the Powell Basin from 29 to 23 Ma using seismic reflection, gravity and magnetic data. They suggest that Powell Basin is a back-arc basin formed as a result of the opening of the Scotia Sea. Using seismic reflection and refraction, ref. [32] proposed a three-phase evolutionary model for the basin: (i) pre-rifting, (ii) rifting, and (iii) oceanic spreading. Also, ref. [34], using multichannel seismic data, proposed three stages with associated ages: (i) a rifting starting at 27 Ma, (ii) an asymmetric spreading of the basin up to 18 Ma generating (iii) the rotation of SOM towards the NE.

Two phases of tectonic evolution, rifting and spreading, have been identified by several authors [7,10,35,36]. Using multichannel seismic profiles and magnetic data, ref. [34] estimated the evolution of the basin happening from the late Eocene (38–34 Ma) to the early Miocene (23–20 Ma). In [36], the scholars proposed a model in which spreading started at 28 Ma and lasted until 17 Ma. Then, active spreading is greatly reduced until its termination at 4 Ma. A spreading period of 29–21 Ma has been suggested [7], with rates of 15–10 km/myr using profiles obtained from a magnetic anomaly grid that were computed from combined aeromagnetic and ship data. A different spreading model with ages of 38–33 Ma and with spreading rates of 17–10 km/myr was proposed by [10].

Several authors have studied the extent of the oceanic crust of Powell Basin. Some authors [7,35] indicate that their models are fully located on the oceanic crust, while [35] suggest a smaller elliptical area in which oceanic spreading develops using magnetic anomalies from a unique marine and multichannel seismic profile dataset. Other authors [33] differentiate three types of crust according to their nature in the Powell Basin, including extended and thinned continental crust, intruded and thinned continental crust, and oceanic

crust (see Figure 6 in [33] and our Figure 2). They proposed an area of oceanic crust in the Powell Basin of a size smaller than those established in previous studies (e.g., [7,34]).

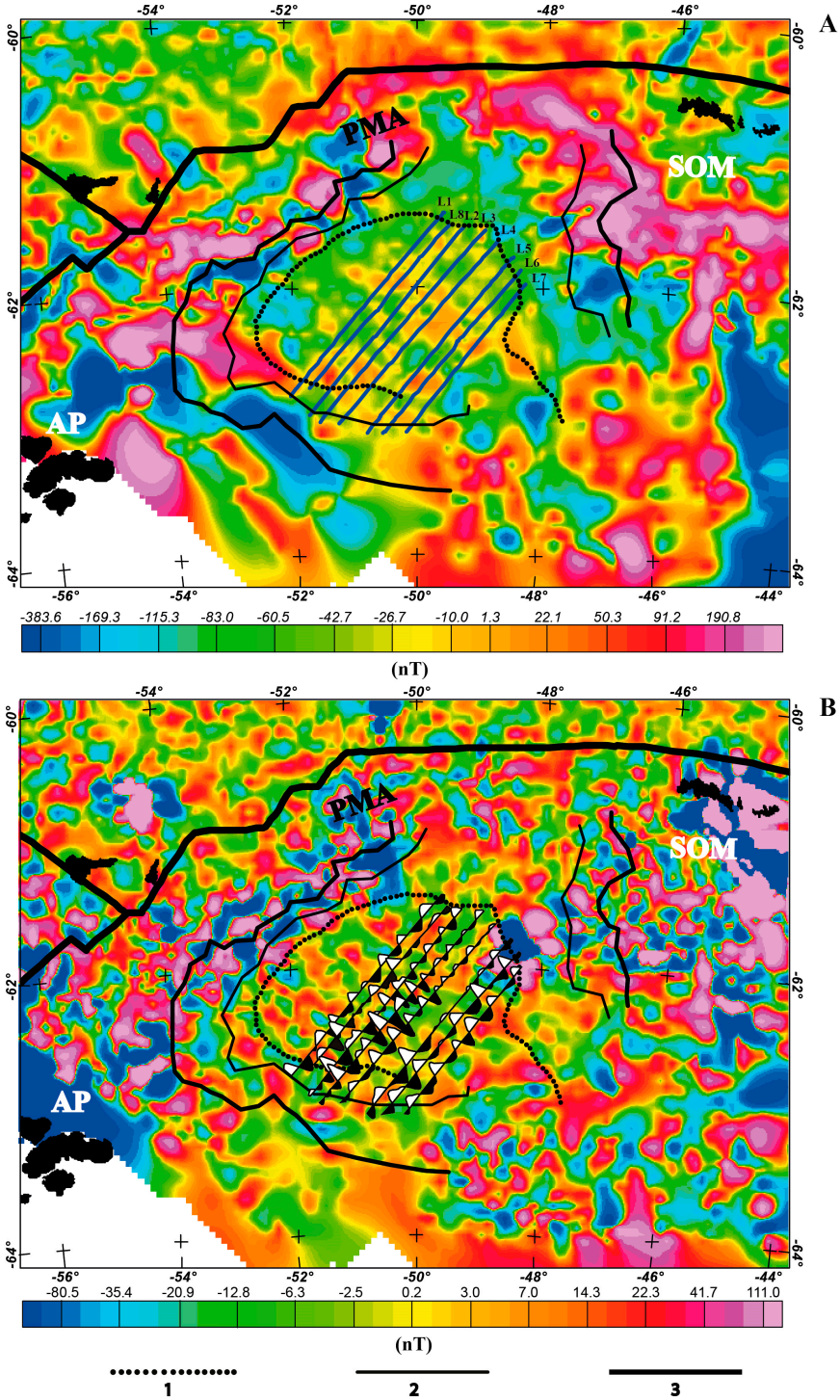

Figure 2. Magnetic signature of the Powell Basin. (**A**) Magnetic anomaly map of the Powell Basin. Blue lines represent the magnetic profiles collected during the ElGeoPoweR expedition. (**B**) Magnetic anomaly map of the Powell Basin high pass filtered 50 km and the magnetic anomaly wiggles identified in each profile. PMA, Pacific Margin Anomaly; SOM, South Orkney Microcontinent; AP, Antarctic Peninsula. 1. Oceanic crust boundary. 2. Intruded and thinned continental crust boundary. 3. Extended and thinned continental crust boundary (boundaries proposed by [33]).

Geothermal heat flow measurements indicate that the spreading phase in Powell Basin ceased at 30.5 Ma [37]. Ref. [20] divided the basin into three areas where they established a correlation between the geothermal heat flow measurements collected during the ElGeoPoweR expedition and crustal magnetization. In addition, ref. [21] correlated geothermal heat flow distribution in the Powell Basin with the existence of an asthenospheric current coming from the Pacific and entering the Scotia and Weddell seas.

The existence of asthenospheric currents during the formation of the Drake Passage and the Scotia Sea have been studied by several authors. Some authors [21] suggest an outflow current from the Pacific mantle through the Drake Passage that flowed freely in the early stages of the formation of the Scotia Sea. Others [18,19] have identified the presence of asthenospheric currents in the Scotia Sea based on gravity and heat flow studies. They have proposed a possible connection of one of these currents with the Weddell Sea through Powell Basin. Magnetic anomaly and geothermal heat flow studies [20,33] indicate the presence of an asthenospheric current in Powell Basin that may represent the connection between the Weddell Sea and the Scotia Sea. Ocean current and climate studies have been conducted in Powell Basin to understand if its formation could have caused regional and global changes. The Weddell Sea Deep Water (WSDW) is observed in the Powell Basin, which is located in the northwestern part of the Weddell Sea [21,38,39]. This deep water mass is part of the Antarctic Bottom Water (AABW) [40]. The AABW is composed of two deep water masses: the Weddell Sea Bottom Water (WSBW) and the WSDW. The WSBW has bathymetric limitations and is only found in the Weddell Gyre, while the WSDW flows above it without limitations and connects with the Scotia Sea [38,40]. These water masses are of great importance since they have a role in controlling and impacting the climate of the surrounding regions during the evolution of the Scotia Arc [41].

Several authors have studied the evolution of ocean currents since the formation of the Drake Passage, as well as its global impact (e.g., [15,17,21,25,38,41–45]). Ref. [17] divided the oceanic basins located in the southern Scotia Sea into two types according to their structural and sedimentary characteristics: external basins (Ona and Scan basins) and internal basins (Protector, Dove, and Pirie Basins). The external basins were formed during the initial stages of the opening of the Drake Passage. This process took place under an ill-defined extensional regime, these basins present a WNW–ESE direction [5,24,43,44]. Ref. [17] established a model of the tectonic evolution and their impact in ocean circulation and climate. They also observed changes in the marine sediments, indicating a regional tectonic change in the evolution of the Scotia Arc in the early Miocene (~22 Ma) that produced a change in the direction from WNW–ESE to W–E for the evolution of the southern basins. Simultaneously, the rifting process in these basins would have ended up with the formation of the internal basins [7,8,46]. Evidence of the WSDW intrusion into the Scotia Sea is observed in the sedimentary record already in the middle Miocene, when the rifting and spreading stages of the inner basins have ended [17]. Some authors [41] have proposed ages of 12.6 Ma in their regional model for this change in the sedimentary record. Other authors [42] have proposed ages from 14.2 to 8.4 Ma by studying the sedimentary record of the IODP 382 expedition for this change. The initial incursions of the WSDW are proposed to happen when the Jane Basin, connecting the Weddell Sea to the Scotia Sea, was fully opened [6].

Simultaneously, the South Scotia Ridge (SSR) passages are open [47,48], and the SFZ started it uplift in the mid Miocene [49]. The formation of the SFZ modified the water masses circulation in the Drake Passage. This favored the onset of thermal isolation in Antarctica and the evolution of Antarctica ice sheets [50]. This setting favored the anticlockwise flow of the WSDW in the area of the SFZ and Ona Basin, connecting it to the Pacific Ocean [17,42,50]. At 8 Ma, the final uplift of the SFZ occurred causing the migration of the CDW to the north (see Figure 1) and splitting the WSDW in two branches, one flowing to the Pacific and one to the north into the Scotia Sea, which increased the thermal isolation of Antarctica [23,49,50].

Sediments belonging to three different climatic stages (pre-glacial, transitional, and glacial regimes) have also been identified in the Powell Basin [16]. Ref. [21] showed the importance of geodynamics in the impacts of ocean current and global climate changes. Therefore, Powell Basin is in a key location to understand the history of the drifting of the SOM and the impact of the formation of the basin within an oceanic gateway.

3. Data and Methodology

In this section, we describe the different datasets used in our study as well as the methodology to perform the ocean spreading models. The integration of different data allows us to better constrain the oceanic spreading models and to determine the history and impact of the Powell Basin.

3.1. Magnetic Data

During the ElGeoPoweR expedition, magnetic data were collected onboard of the R/V Sarmiento de Gamboa using a SeaSpy 300 magnetometer from the Spanish Research Council. A total of eight magnetic profiles (Figures 1B and 2) were performed in Powell Basin. The profiles were SW–NE oriented, perpendicular to the spreading axis, and of an approximate length of 200 km each. The acquired data were then combined with existing profiles [51,52] to produce a new magnetic anomaly map of the area (Figure 2A).

Corrections were applied to the magnetic data once we obtained the position of the sensor with respect to the ship. These corrections included (i) the diurnal variation to remove the contribution of external magnetic fields using data from a nearby magnetic observatory in Livingston Island, (ii) the subtraction of the contribution of the core field using the IGRF 13 model [53], and (iii) leveling corrections by applying a leveling algorithm [54] to reduce positioning errors and obtain a corrected map.

Once we performed all corrections, we integrated data from previous surveys [51] included in the World Digital Magnetic Anomaly Map (WDMAP) v2 [52] to create a new magnetic anomaly grid of Powell Basin. To improve the coherence between the WDMAM v2 data and our new marine magnetic data, we worked on leveling to obtain a magnetic anomaly map of the Powell Basin (Figure 2A). Later, we used a 1D high-pass filter with 50 km as the cutoff wavelength to better discriminate the contribution of subsurface sources (Figure 2B).

3.2. Gravity, Bathymetry, and Sediment Thickness Data

We used the global free air dataset with a 1-mile resolution [55] (Figure 3) to understand the horizontal distribution of subsurface bodies. This allowed us to better constrain the location of the extinct spreading axis in Powell Basin. The SRTM30plusv7 grid with a 1-km resolution [56] was used for the seafloor topography. We used the sediment thickness grid (see Figure 3C of [33]) obtained from the multichannel seismic profiles in Powell Basin.

3.3. Oceanic Spreading Modeling

We used Modmag software v1 [57] to create the oceanic spreading models. For this purpose, we used the magnetic anomaly profiles collected during our expedition and selected certain spreading rates for each evolutionary period during the evolution of the basin. The spreading direction is represented by the actual position of each profile with respect to the north since each was perpendicular to the ridge. We used the boundaries proposed by [33] to locate the ocean–continent boundaries in the region and constrain the ocean-related magnetic anomalies. The spreading axis was identified using gravity and bathymetry data [33,56]. The Ogg Geomagnetic time scale [58] was used for age assignment.

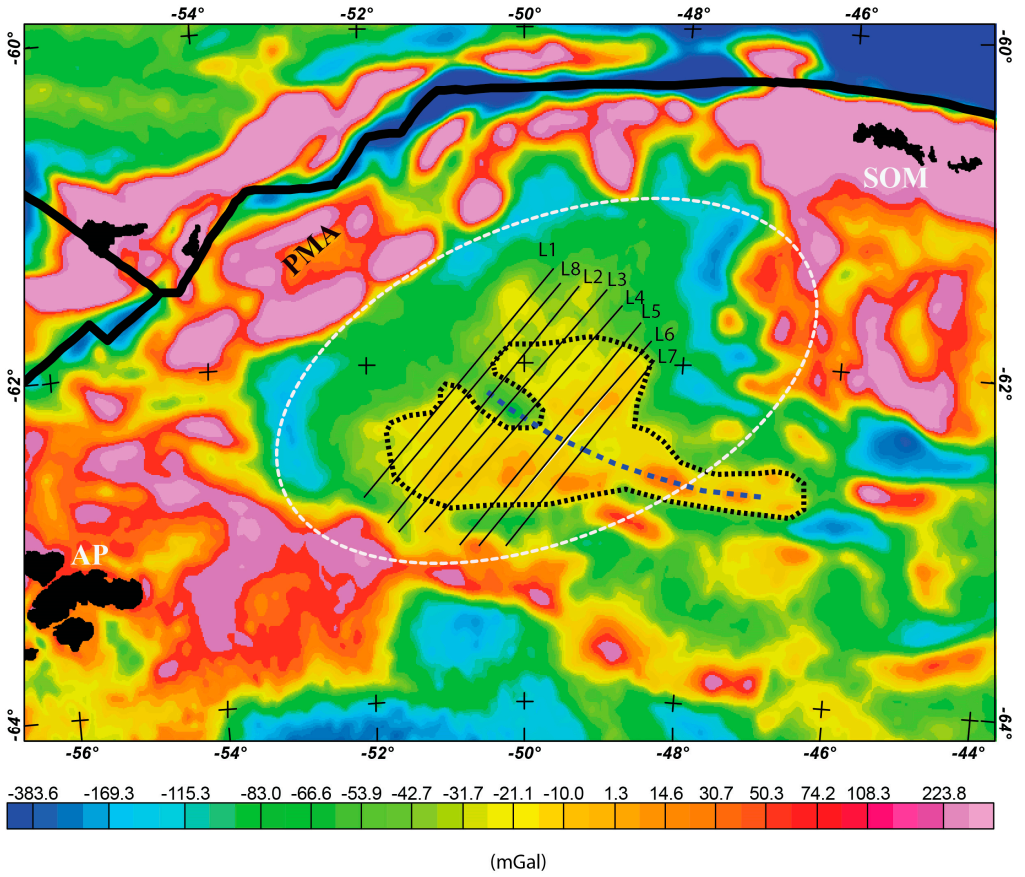

Figure 3. Free-air gravity map of the Powell Basin. The white dash line defines the geological boundaries of the Powell basin. The black dashed line shows a Y-shaped anomaly high in the center of the basin. The blue dashed line represents the position of the extinct spreading axis. The black lines indicate the position of the magnetic profiles. PMA, Pacific Margin Anomaly; SOM, South Orkney Microcontinent; and AP, Antarctic Peninsula.

The structure of the oceanic crust is represented by two main magnetic layers [33]. The upper layer, called layer 2A [59], is formed by titanomagnetite and presents a thickness of less than 1 km. The lower layer is formed by dolerites and gabbros and presented a thickness of 5 km [60]. Both layers contribute to the magnetic response, but only the upper layer is responsible for the magnetic anomalies [61,62]. The magnetic layer that was used in our model and was responsible for the observed magnetic anomalies was considered to be 500-m thick starting at the top of the basement. Its topography was calculated based on the sediment thickness obtained from multichannel seismic profiles from the Seismic Data Library System (https://scar.org/library-data/data/seismic-data, (accessed on 5 August 2024) located in the Powell Basin and the seafloor bathymetry [33,56].

4. Results

4.1. Magnetic Signature of the Powell Basin

The magnetic anomaly map (Figure 2A) provides the opportunity to study the basin by analyzing the amplitudes of the magnetic anomalies. Relatively short-wavelength and low-amplitude anomalies characterize the central part of the basin. On the other hand, the areas characterized by long-wavelength magnetic anomalies are in the northern and western parts of the Powell Basin, which are associated with the PMA [63].

The filtered magnetic anomaly map (Figure 2B) allows us to investigate and differentiate the anomalies in each profile and compare their amplitudes. This map also helps us to locate the anomalies in the specific type of crust observed in the Powell Basin [33]. The anomalies with higher amplitudes correspond to locations at the ends of profiles, coinciding

with areas of continental crust. Anomalies with intermediate amplitudes are found in the continental–oceanic crust transition zones, and the lowest amplitudes characterize the central part of the basin.

4.2. Position of the Extinct Spreading Axis

Some authors [35] have identified the spreading axis in the Powell basin; it is divided into two ridges separated by a depression filled with sediments. The free-air gravity anomaly map (Figure 3) allows us to locate the position of the extinct spreading axis by analyzing the gravity values in the basin. The map shows moderate values (30–40 mGal) for the area identified as oceanic crust [33]. Here, we identify a Y-shaped high anomaly with two trends: (1) W–E presenting higher gravity values, which is in agreement with the area where the magnetic anomalies of higher amplitudes are found, and (2) NW–SE trend showing lower gravity values in the NW increasing toward the center of the feature. The NW part coincides with the position of the low-amplitude magnetic anomalies. The space between them marks the extinct spreading axis (see the blue dashed line in Figure 3).

The sediment thickness map (see Figure 3C in [33]) indicates that the sediment thickness layer is thinner where the extinct spreading axis is located.

4.3. Oceanic Spreading Model

The filtered magnetic anomaly map of the Powell Basin (Figure 2B) is used to develop the oceanic spreading models. This map allows us to detect the magnetic responses of the layers that generate ocean floor anomalies with higher accuracies.

We use eight magnetic profiles (L1, L8) obtained in Powell Basin (Figure 2) to elaborate an oceanic spreading model. The profiles are SW–NE oriented and are perpendicular to the spreading axis. The profiles are projected perpendicular to the anomaly strike with a N45°E direction with respect to the geographic north. Our spreading model considers the oceanic crust boundary proposed by [33] (see Figure 2A).

The differences between the spreading rates, the number of anomalies, and their amplitudes in each profile and throughout the basin indicate that the evolutions in the Powell Basin are different in the north and south. This is the basis for us to propose two different evolution models: one for the north and one for the south (Figures 4 and 5).

For the north (profiles L1, L8, L2, L3, L4), we propose a spreading model between 38.08 Ma (Chron C17) and 21.8 Ma (Chron C6AA) with spreading rates ranging from 13 to 5 km/myr. In this area, we have identified a number of anomalies on both sides of the extinct axis for each profile (see Figure 4). In the south (profiles L5, L6, L7), and based on the number of observed magnetic anomalies, we obtain a spreading model from 38.08 Ma (Chron C17) to 25.2 Ma (Chron C8) with spreading rates ranging from 10 to 5 km/myr (Figure 5).

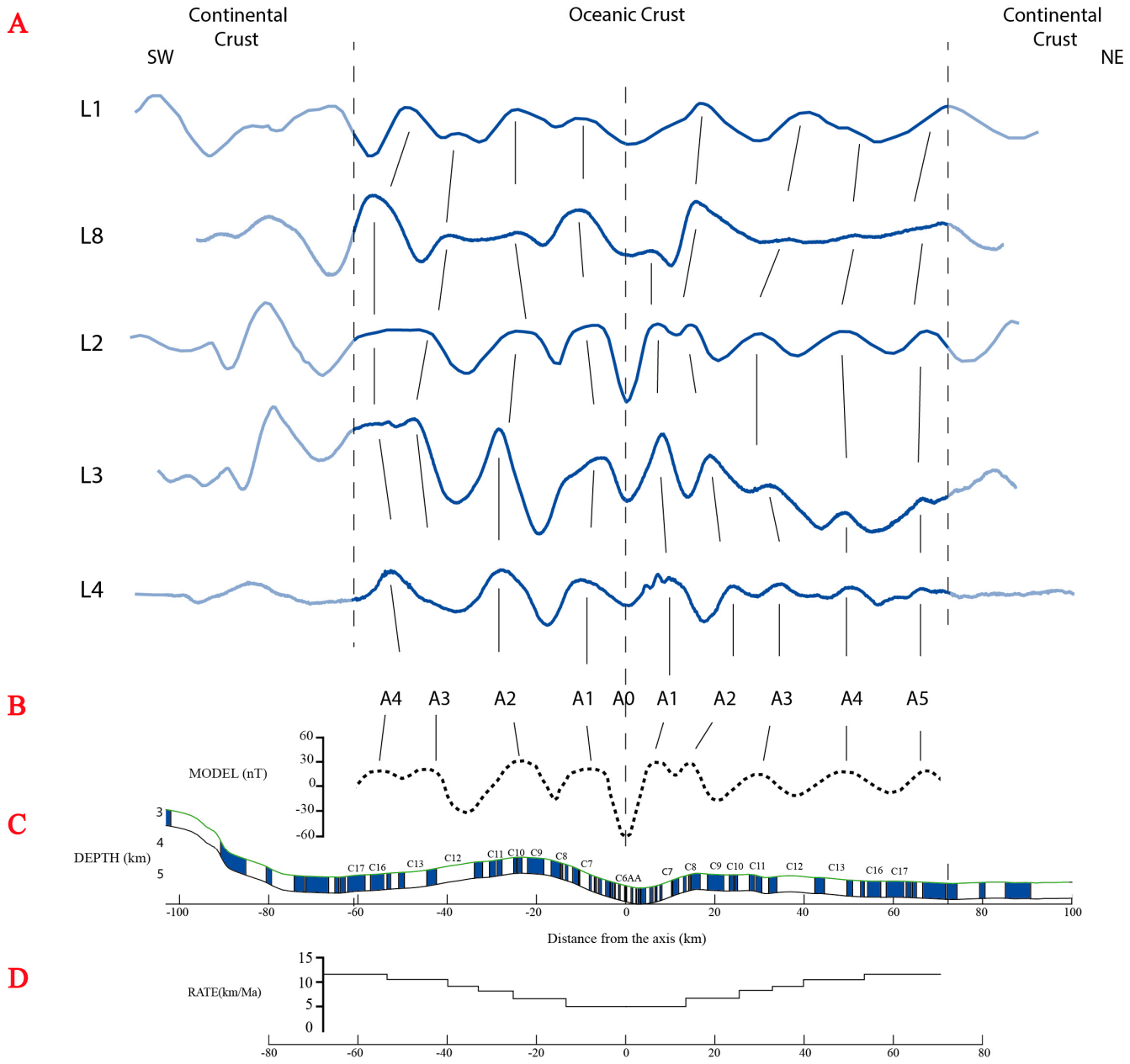

Figure 4. Oceanic spreading model based on magnetic anomalies for the northern part of the Powell Basin. (**A**) Magnetic profiles of Powell Basin (see Figure 2A for location). The light blue colors represent the sections of the magnetic profiles where the anomalies are situated outside the oceanic crust. This part of the profiles has not been used for modeling. The dashed vertical lines indicate the limits of the oceanic crust. (**B**) Synthetic spreading model for 38.08–21.8 Ma. A0 corresponds to the position of the extinct spreading axis. The identified anomalies are labeled as A. (**C**) Representation of the magnetic layer of profile L3 including the basement topography and a thickness of 0.5 km. Assigned Chrons are indicated here. (**D**) Spreading rates.

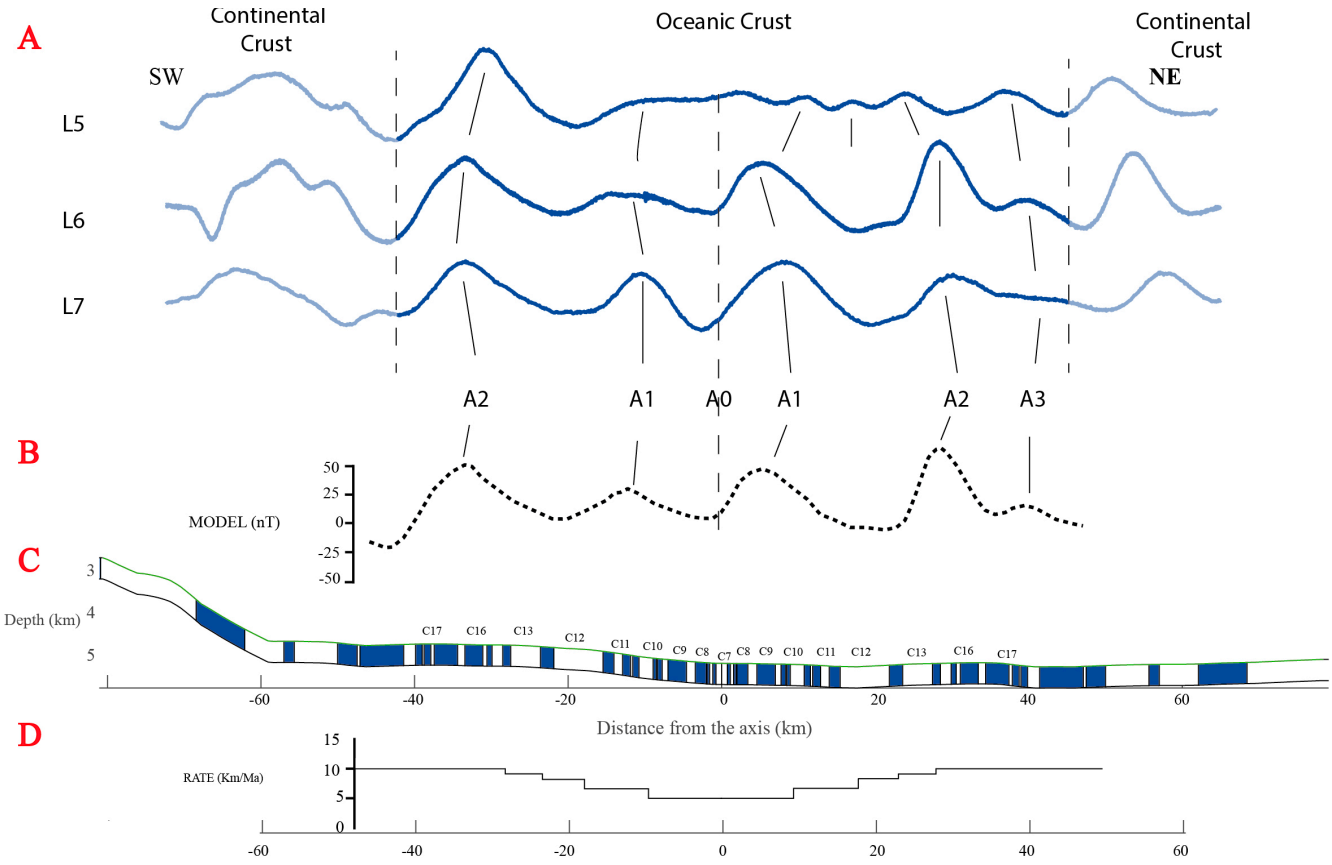

Figure 5. Oceanic spreading model based on magnetic anomalies in the southern part of the Powell Basin. (**A**) Magnetic profiles of the Powell Basin (see Figure 2A for location). The light blue colors represent the sections of the magnetic profiles where the anomalies are situated outside the oceanic crust. This part of the profile has not been used for modeling. The dashed vertical lines indicate the limits of the oceanic crust. (**B**) Synthetic spreading model for 38.08–25.2 Ma. A0 corresponds to the position of the extinct spreading axis. The identified anomalies are labeled as A. (**C**) Representation of the magnetic layer of profile L3 including the basement topography and a thickness of 0.5 km. Assigned Chrons are indicated here. (**D**) Spreading rates.

5. Discussion

Our data and oceanic spreading models, together with additional geophysical information (e.g., heat flow, gravity anomalies, and sediment thickness) from other authors [20,33], provide new insights into the formation and evolution of the Powell Basin.

5.1. Oceanic Spreading and the Evolution of the Powell Basin

Our recent magnetic anomaly data as well as our proposed oceanic spreading model support a different timing for the evolution of the north and south parts of the Powell Basin. The northern part of the basin evolved during a longer period (38.08–21.8 Ma) of time than the south (38.08–25.2 Ma).

The difference in the numbers, spreading rates, and amplitudes of the anomalies between the northern and southern parts of the Powell Basin help us to establish a different symmetric model for each area. We also observe that there are differences when analyzing the spreading rates geographically within the basin.

First, we analyze the spreading rates on both sides of each profile. We select pairs of anomalies located in the oceanic crustal zones on both sides of each profile of a similar age. By locating the position of the highest value of each anomaly with respect to the center of the spreading zone in each profile (Table 1), we obtain its distance to the axis. This way, we compare the spreading rates for the same anomalies on both sides of the spreading

axis to understand possible asymmetries. This allows us to identify the process that may have affected the development of the basin in both regions. We observe notable differences between profiles in the same area (north or south) and between the two areas. The profiles located in the northern part (L1, L8, L2, L3, L4) show larger differences in the spreading rates compared to the profiles in the south. This difference is observed between profiles L3 from the north and L6 from the south, where L3 presents a spreading rate value of 15.4 km/myr in anomaly A4 and profile L6 presents a value of 10.8 km/myr in anomaly A2 (Table 1). However, these anomalies represent the same Chron, C17n (38.08 Ma). We also observe differences in spreading rates within the same profile in the northern part depending on its location with respect to the spreading axis. An example of this is observed in profile L3; for the same anomaly (A4, see Table 1), we obtain different spreading rates at both sides of the spreading axis: 14.2 km/myr on the east side and 15.4 km/myr on the west (Table 1).

Table 1. The positions of the magnetic anomalies in each profile that are clearly recognized in the oceanic crust at both sides of the spreading axis. The distance refers to the absolute distance from the axis to the position of each anomaly. The Δ distance is the distance between the clearly recognized consecutive highs. The spreading rates are the values obtained for these anomalies. Asymmetry is the difference between the spreading rates of the same magnetic anomaly at both sides of the spreading axis.

	West Ridge Part				East Ridge Part				
Profile	**Anomaly**	**Distance (km)**	**Δ Distance (km)**	**Spreading Rate (km/myr)**	**Anomaly**	**Distance (km)**	**Δ Distance (km)**	**Spreading Rate (km/myr)**	**Asymmetry (%)**
L1	A1	11	11	4.2	A1	15	15	5.5	13
	A2	26	15	8.3	A2	38	23	10.8	25
	A3	40	14	11.4	A3	48	10	12.9	15
	A4	55	15	14.8	A4	71	23	19	42
L8	A1	8	8	3.3	A1	5	5	2.1	12
	A2	18	10	6.8	A2	15	10	5.5	13
	A3	39	21	11.8	A3	36	21	11.2	6
	A4	55	16	15.2	A4	50	14	14.2	10
L2	A1	10	10	4	A1	5	5	2.1	19
	A2	23	13	7.9	A2	14	9	5.3	26
	A3	45	22	12.8	A3	30	16	9.6	32
	A4	55	10	15.2	A4	48	18	12.9	23
L3	A1	9	9	4	A1	8	8	3.6	4
	A2	28	19	9.5	A2	19	11	7.5	20
	A3	46	18	13.6	A3	32	13	10.3	33
	A4	55	9	15.4	A4	48	16	14.2	12
L4	A1	10	10	4	A1	8	8	3.3	7
	A2	27	17	7.9	A2	22	14	6.6	13
	A3	52	25	14.3	A3	34	12	9.7	46
L5	A1	13	13	4.4	A1	12	12	4.2	2
L6	A1	12	12	4.3	A1	12	12	4.3	0
	A2	40	28	10.8	A2	40	29	10.8	0
L7	A1	12	12	4.1	A1	13	13	4.3	2
	A2	38	26	10.2	A2	38	38	10.2	0

For the profiles in the south (L5, L6, L7), we observe symmetry in the spreading rates at both sides of the spreading axis. An example is observed in profile L6 where we obtain the same spreading rates for all the anomalies located in this profile on both sides of the spreading axis (Table 1).

We also compare the number of magnetic anomalies observed in the same profile at both sides of the spreading axis and between profiles. The magnetic profiles obtained

in the northern part of the basin are longer than those in the south, and the number of magnetic anomalies observed in the north and the south differ. To compare both areas and analyze the differences, the number of anomalies located on the oceanic crust in each profile (oceanic spreading magnetic anomalies of each profile) is obtained (Table 2). For this purpose, the magnetic anomaly highs are selected in each profile (white part of the wiggle in each profile, see Figure 2B). The northern profiles show a higher number of anomalies (8–9) than those located in the south (5–6) (see Table 2). Our results agree with those from previous studies [7,33] regarding notable differences in the amplitudes of the magnetic anomalies. We observe that the anomalies located in the north present lower amplitudes than those in the south (Figure 2B).

Table 2. Number of anomalies identified in each magnetic profile and the total length of each profile.

Profile	Nº Anomalies	Oceanic Anomalies	Profile Length (KM)
L1	11	8	200
L8	11	9	180
L2	12	9	203
L3	13	9	212
L4	10	8	202
L5	8	6	190
L6	7	5	179
L7	8	5	160

We find clear differences between the spreading rates of the northern and southern profiles (Table 1). In the profiles located in the northern region, we observe an asymmetry percentage of ~10% for anomalies close to the spreading axis. The asymmetry percentage increases to values of ~35% in anomalies close to the continental crust. The values in the southern profiles do not show asymmetry. Some of the spreading rate asymmetry can occur due to the intrinsic error of picking the location of the high in each anomaly. We consider that if the spreading rate differences are larger than 10%, the asymmetry likely exists

These results allow us to interpret an evolutionary model for the northern part of the basin that is more complex than in the southern part. The main cause is the higher number of anomalies and the loss of magnetization in the eastern part of each northern profile. The loss of magnetization implies a modification of the magnetic response in the oceanic crust during the process of the evolution of the basin. The southern part is interpreted as a stage of greater tectonic calm due to the symmetry between the numbers, amplitudes, and spreading rates of the anomalies. The higher numbers of magnetic anomalies in the northern region (Table 2) indicate a longer spreading period for this area.

In addition, our synthetic models also differ from those proposed by other authors in the past. Some reasons for the main differences are the orientation and kind of data (data points vs. grided data) used to build the models. The model proposed by [7], hereafter referred to as EL2002, generated the model extracting profiles from a magnetic anomaly grid with an SSW–NNE orientation. While [10], hereafter referred to as SC2022, generated the models using magnetic profiles and one seismic line. The orientations of the models from SC2022 and from EL2002 are the same. Our data come from the profiles themselves and are SW-NE oriented. Our data provide us with the opportunity to better observe the trends of anomalies and the asymmetries in the spreading axis and to better constrain our evolution model.

In order to understand the different timings and evolutions for Powell Basin, we compare the data and models proposed by other authors [7,10] with ours (Figure 6). The comparison with the EL2002 model is as follows. First, we identify the profiles they used to build their model. This allows us to identify the length of each profile, the position of each of the magnetic anomalies in the respective profile and their geographic location within

the basin (see Figure 3B in [7]). We note that the profiles considered for our model in the northern area of Powell Basin coincide with the geographical position of EL2002, which allows us to make a detailed comparison between the two models. Later, we check if all the ocean spreading magnetic anomalies proposed in their model are within the oceanic crust boundaries defined by [33] as we use these boundaries to constrain our model.

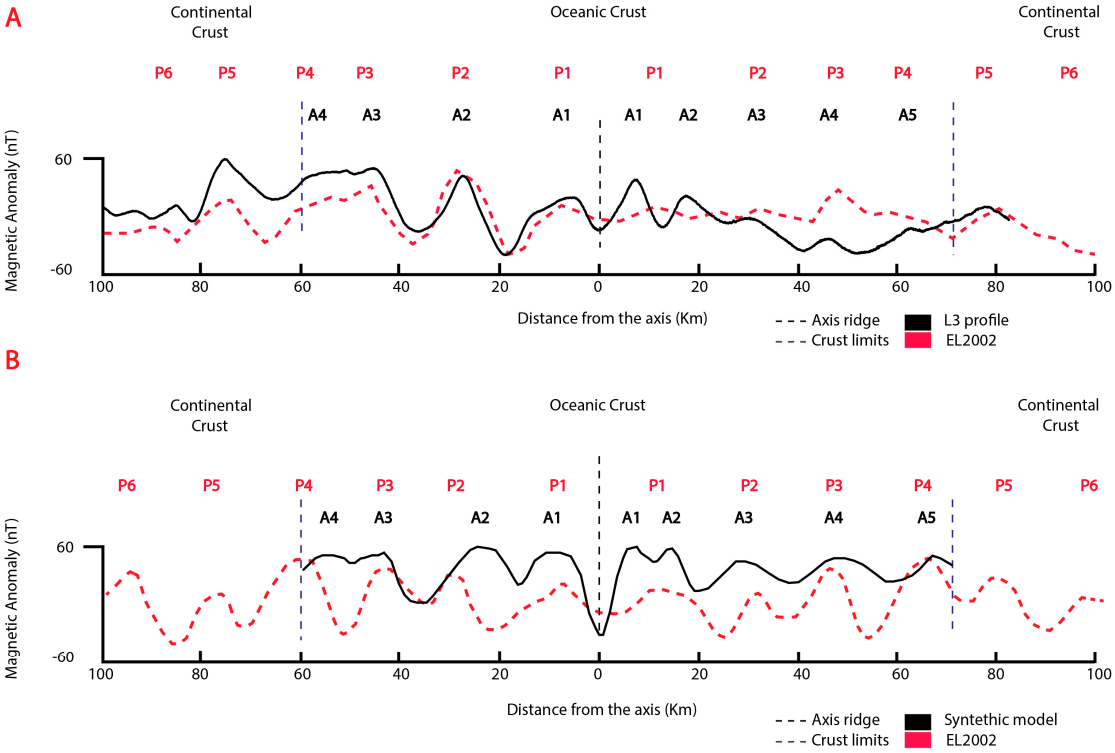

Figure 6. Comparison of EL2002 and our models. (**A**) Comparison of the positions of the magnetic anomalies in our profile L3 located in the northern area with the profile from EL2002. (**B**) Comparison of the positions of the magnetic anomalies obtained in the synthetic oceanic spreading models. The red dashed line represents the anomalies from the EL2002 synthetic model and their southern profile. The black line is our model. P1–P6 are the magnetic anomalies set in the profile from EL2002 and the synthetic model. A1–A5 are the magnetic anomalies set in our synthetic model of the Powell Basin (Figure 4). The blue dashed vertical lines mark the boundaries between different types of crust (Figure 2A). The gray dashed vertical line indicates the position of the extinct spreading axis for both models.

First, we compare the magnetic anomaly signal derived from one of our profiles with a profile of EL2002, and we then compare both synthetic models (Figure 6A,B). For the comparison of the individual profiles, we use our profile L3. We selected this profile because it shares the position of the extinct spreading axis with one of the profiles from the EL2002 model. This allows us to compare the magnetic anomalies of both models (Figure 6A). We note that the anomalies P5 and P6 of the EL2002 model correspond to the continental crustal zones according to [33]. Within the oceanic crust, we observe a strong correlation between the numbers and positions of the anomalies of EL2002 and ours (A1–A4 and P1–P4) on the west side of the spreading axis. On the other hand, east of the spreading axis, we observe large differences: EL2002 identifies 4 anomalies (P1–P4) while we identify 5 (A1–A5); we cannot establish a good correlation for this area of the basin.

Finally, if we compare the synthetic models (Figure 6B), we find that the anomalies P5 and P6 can modify the result in an oceanic spreading model. The anomaly P5 is located in continental crust in the western part and in the boundaries between oceanic and continental crust in the eastern part. This makes us doubt the nature of these anomalies. The anomaly

P6 is located in continental crust. The position of P6 indicates that it does not belong to the oceanic crust based on the boundaries proposed by [33]. In addition, only a small number of anomalies of the EL2002 model are located in the area proposed to be oceanic crust on both sides of the spreading axis. The EL2002 model identifies four anomalies, P1–P4, while we identify five, A1–A5, east of the extensional axis. Both models obtain fewer anomalies (P1–P3) and (A1–A4) in the western part. However, we can also establish a good correlation between several anomalies proposed in the eastern part for both models: P2 with A3, P3 with A4, and P5 with A5.

We also make a similar comparison with the model SC2022. In this case, the spreading axis is not established in the same location as the one in our model. The SC2022 model proposes the spreading axis to be toward the NE with respect to our model (see Figure 5 in [10]). We determine that their oceanic spreading anomalies are located in continental crust or transition zones based on the crustal boundaries proposed by [33].

We compare the extent of oceanic crust in Powell Basin considered by other authors (e.g., [7,10,32]) with the one used to constrain our model [33]. We observe that the oceanic crust limits proposed by previous authors are different from those proposed by [33]. We consider that the anomalies that are located outside our oceanic crust limits do not correspond to oceanic spreading magnetic anomalies, but rather correspond to fractures around the extension close to the oceanic crust. Therefore, they present rifting fractures through which magma exited, and they do not represent oceanic spreading magnetic anomalies that can be used for modeling to accurately understand the history of the spreading in Powell Basin. The existence of anomalies outside our limits of oceanic crust in the models proposed by other authors (e.g., [7,10]) may be due to the different orientations in the profiles. These are not perpendicular to the spreading axis and therefore do not strictly follow spreading corridors, potentially crossing fracture zones. This is a source of uncertainty about the assigned ages for the evolution of the basin, supporting the need to establish additional stages for the spreading of the basin.

The seismic data presented by [32] in Powell basin do not identify a structure at the bottom of the basin that differentiates the north and the south, but they allow the authors to define the oceanic crustal region. Some authors [33] have identified the tectonic boundaries of the Powell Basin and established a subdivision of the nature of the crust comprising basin. The differences in the number of magnetic anomalies and the amplitudes between the southern and northern profiles indicate that the evolutionary processes are different in the southern and northern regions. We propose a zipper spreading model starting from a common point located in the eastern part of the spreading axis. This model explains the age difference between the southern and northern parts of the basin without the need of a structure, like a transfer zone or fault, in the center of the basin.

5.2. Impacts of the Evolution of the Powell Basin

Our magnetic anomaly data obtained during our last cruise show higher amplitudes ($\pm$25 nT) in the southern part of Powell Basin that are coincident with the region of relatively high-gravity anomaly values. Lower magnetic anomaly amplitudes ($\pm$10 nT) are observed in the NE part of the basin where the lowest gravity values are found (Figures 3–5). The variation in the magnetic response of the oceanic crust can be explained by two factors: hydrothermal circulation and heat. Some authors [7,32] indicate that the lower amplitudes of the magnetic anomalies correspond to a hydrothermal alteration process. Sediment thickness data from the Powell Basin (see Figure 3B in [20]) show constant values throughout the basin, so we believe that it is not an adequate factor to explain the amplitudes of the magnetic anomalies. Other authors [20] have proposed that the magnetization signature as well as the geothermal heat flow values are driven by the presence of an underlying asthenospheric flow. These authors have also obtained higher heat flow values (105–117 mW/m^2) in the northeastern part of Powell Basin coinciding with the area where we and other authors (e.g., [7,32]) identify low-amplitude magnetic anomalies (35–40 nT). Also, geothermal heat flow values decrease toward the south of

Powell Basin (66 mW/m^2), coinciding with the areas where the amplitudes of the magnetic anomalies are higher.

The age proposed in our model for the onset of the oceanic crust in Powell Basin is 38.08 Ma (Eocene). From this age until the Oligocene, Antarctica and South America were breaking up, which led to the formation of the Drake Passage and the Scotia Sea [25,45]. The Drake Passage formed as a consequence of the eastward movement of the Scotia Arc since the Oligocene (34 Ma) [6,26,64]. The opening of the Drake Passage favored the future development of the Scotia Sea. Several authors have studied the origin of oceanic crust in the Scotia Sea and agree that oceanic crust has existed for at least 28 Ma (e.g., [65,66]). Some authors [26] propose an older onset of oceanic crust of around 32 Ma in the Scotia Sea.

We consider the intrusion of an asthenospheric and oceanic current into the Powell Basin to be related to the separation of the SOM from the Antarctic Peninsula. We also believe that the development of a new ocean floor due to the onset of spreading in Powell Basin may have facilitated the southern intrusion of oceanic currents from the Weddell Sea at 38 Ma. According to the models of the Powell Basin evolution from other authors (e.g., [7,34]), the migration of the SOM started in the Oligocene (32 Ma). The existence of low-amplitude magnetic anomalies makes it difficult to establish more accurate age models for the evolution of Powell Basin. In addition, the separation of the SOM and the formation of oceanic basin produce lithospheric thinning that facilitates the incursion of the asthenospheric current from the Scotia Sea into the Powell Basin.

We consider that the asthenospheric current incursion into Powell Basin occurred at least 28 Ma, when oceanic crust in the Scotia Sea is identified by a number of authors (e.g., [26,66,67]). Also, ref. [16] established the change from a pre-glacial climatic regime to a transitional regime in Powell Basin at 27 Ma and we propose the end of the oceanic spreading of the south part of Powell Basin at 25.2 Ma.

From the Oligocene to the Early Miocene, the Scotia Sea continued to form simultaneously with the formation of the external basins, Ona and Scan [17,42]. The formation of the oceanic crust associated with the evolution of these basins continued to facilitate the incursion of the asthenospheric flow into the Powell Basin.

In the Early Miocene (~22 Ma), the beginning of the intrusion of the WSDW into the Scotia Sea may have occurred [17,42]. This took place with the final stage of spreading of the Powell Basin in the northern area. Based on the sedimentary record, the intrusion of the WDSW into the Scotia Sea occurred in the middle Miocene [17].

6. Conclusions

The integrated approach of new magnetic data with existing gravity, geothermal heat flow, and sediment thickness data contribute to a better understanding of the geodynamic evolution of Powell Basin. We propose a new oceanic spreading model using recent magnetic data that is fully enclosed within the oceanic crust as opposed to the previous proposed models (e.g., [7,10]).

The differences between the spreading rates, numbers, and amplitudes of anomalies in each profile and throughout the basin indicate that the evolution of the Powell Basin was asymmetric between the north and the south. In the southern part (profiles L5, L6, L7), our model suggests ages from the late Eocene (38.08 Ma) to the late Paleogene (25.2 Ma). In the north (profiles L1, L8, L2, L3, L4), the model presents ages from the late Eocene (38.08 Ma) to the early Miocene (21.8 Ma).

According to our models, we consider that asthenospheric currents flowed into the Powell Basin just after the opening of the Drake Passage, and we consider the existence of oceanic crust in the Scotia Sea (~28 Ma) (e.g., [26,65,66]), weakening the oceanic spreading magnetic anomalies and impacting the magnetization of the new ones. The intrusion of oceanic currents from the Weddell Sea into the Powell Basin likely started at the time of oceanic crust generation in the basin.

Author Contributions: M.C. and Y.M.M. designed the experiment. A.S.B., M.C. and Y.M.M. processed and interpreted the magnetic and gravity data. A.S.B. and Y.M.M. drafted the manuscript. All authors have read and agreed to the published version of the manuscript. All authors listed have made a substantial and intellectual contribution to the work and approved it for publication.

Funding: This study was funded by project RTI 2018-099615-B-100 "Estructura Litosférica y Geodinámica de Powell Drake-Bransfield Rift" funded by the Spanish Government. Y.M. was also supported by NASA under award number 80GSFC21M0002 and 80GSFC24M0006.

Data Availability Statement: Results will be made publicly available at the time of publication in Zenodo (link TBD).

Acknowledgments: All authors would like to thank the support of the crew of the R/V Sarmiento de Gamboa during the "ElGeoPoweR" Antarctic expedition. The authors thank the reviewers for their constructive comments and suggestions. We also would like to thank Graeme Eagles for sharing his materials from the EL2002 model that greatly helped us with the discussion of our study. A.S.B. and Y.M.M. will never forget Manen Catalán's passion for science and would like to dedicate this manuscript to him.

Conflicts of Interest: The authors declare no conflicts of interest.

References

1. Wilson, J.T. Continental Drift. *Sci. Am.* **1963**, *208*, 86–103. [CrossRef]
2. Heirtzler, J.R.; Dickson, G.O.; Herron, E.M.; Pitman, W.C., III; Le Pichon, X. Marine magnetic anomalies, geomagnetic field reversals, and motions of the oceanic floor and continents. *J. Geophys. Res.* **1968**, *73*, 2119–2136. [CrossRef]
3. Meyerhoff, A.A. Continental drift: Implications of paleomagnetic studies, meteorology, physical oceanography and climatology. *J. Geol.* **1970**, *78*, 1–51. [CrossRef]
4. Bohoyo, F.; Galindo-Zaldívar, J.; Maldonado, A.; Schreider, A.A.; Suriñach, E. Basin development subsequent to ridge-trench collision: The Jane Basin, Antarctica. *Mar. Geophys. Res.* **2002**, *23*, 413–421. [CrossRef]
5. Eagles, G.; Jokat, W. Tectonic reconstructions for paleobathymetry in Drake Passage gateway. *Tectonophysics* **2014**, *611*, 28–50. [CrossRef]
6. Ryan, W.B.; Carbotte, S.M.; Coplan, J.O.; O'Hara, S.; Melkonian, A.; Arko, R.; Weissel, R.A.; Ferrini, V.; Goodwillie, A.; Nitsche, F.; et al. Zemsky. Global Multi-Resolution Topography synthesis. *Geochem. Geophys. Geosyst.* **2009**, *10*, Q03014. [CrossRef]
7. Eagles, G.; Livermore, R.A. Opening history of Powell Basin, Antarctic Peninsula. *Mar. Geol.* **2002**, *185*, 195–205. [CrossRef]
8. Galindo-Zaldívar, J.; Bohoyo, F.; Maldonado, A.; Schreider, A.; Surinach, E.; Vázquez, J.T. Propagating rift during the opening of a small oceanic basin: The Protector Basin (Scotia Arc, Antarctica). *Earth Planet. Sci. Lett.* **2006**, *241*, 398–412. [CrossRef]
9. Galindo-Zaldívar, J.; Puga, E.; Bohoyo, F.; González, F.J.; Maldonado, A.; Martos, Y.M.; de Federico Antonio, D. Reprint of "Magmatism, structure and age of dove basin (Antarctica): A key to understanding south scotia arc development". *Glob. Planet. Chang.* **2014**, *123*, 249–268. [CrossRef]
10. Schreider, A.A.; Sazhneva, A.E.; Kluyev, M.S.; Brekhovskikh, A.L.; Bohoyo, F.; Galindo-Zaldivar, J.; Evsenko, E.I. Kinematic Model of the Development of the Bottom of the Powell Basin (Weddell Sea). In *Processes in GeoMedia—Volume V*; Springer: Cham, Switzerland, 2022; pp. 197–207. [CrossRef]
11. Garrett, S.W.; Renner, R.G.B.; Jones, J.A.; McGibbon, K.J. Continental magnetic anomalies and the evolution of the Scotia Arc. *Earth Planet. Sci. Lett.* **1987**, *81*, 273–281. [CrossRef]
12. Maslanyj, M.P.; Garrett, S.W.; Johnson, A.C.; Renner, R.G.; Smith, A.M. *Aeromagnetic Anomaly Map of Western Antarctica (Weddell Sea Sector)*; Scale 1:2 500,000; British Antarctic Survey: Cambridge, UK, 1991; *BAS* GEOMAP Ser, Sheet 2.
13. Martos, Y.M.; Catalán, M.; Galindo-Zaldívar, J.; Maldonado, A.; Bohoyo, F. Insights about the structure and evolution of the Scotia Arc from a new magnetic data compilation. *Glob. Planet. Chang.* **2014**, *123*, 239–248. [CrossRef]
14. King, E.C.; Barker, P.F. The margins of the south Orkney microcontinent. *J. Geol. Soc.* **1988**, *145*, 317–331. [CrossRef]
15. Galindo-Zaldívar, J.; Balanyá, J.C.; Bohoyo, F.; Jabaloy, A.; Maldonado, A.; Martınez-Martınez, J.M.; Suriñach, E. Active crustal fragmentation along the Scotia–Antarctic plate boundary east of the South Orkney Microcontinent (Antarctica). *Earth Planet. Sci. Lett.* **2002**, *204*, 33–46. [CrossRef]
16. Lindeque, A.; Martos, Y.M.; Gohl, K.; Maldonado, A. Deep-sea pre-glacial to glacial sedimentation in the Weddell Sea and southern Scotia Sea from a cross-basin seismic transect. *Mar. Geol.* **2013**, *336*, 61–83. [CrossRef]
17. Pérez, L.F.; Hernández-Molina, F.J.; Lodolo, E.; Bohoyo, F.; Galindo-Zaldívar, J.; Maldonado, A. Oceanographic and climatic consequences of the tectonic evolution of the southern scotia sea basins, Antarctica. *Earth-Sci. Rev.* **2019**, *198*, 102922. [CrossRef]
18. Martos, Y.M.; Galindo-Zaldívar, J.; Catalán, M.; Bohoyo, F.; Maldonado, A. Asthenospheric Pacific–Atlantic flow barriers and the west Scotia ridge extinction. *Geophys. Res. Lett.* **2014**, *41*, 1–7. [CrossRef]
19. Martos, Y.M.; Catalán, M.; Galindo-Zaldívar, J. Curie depth, heat flux and thermal subsidence studies reveal the Pacific mantle outflow through the Scotia Sea. *J. Geophys. Res. Solid Earth* **2019**, *124*, 10735–10751. [CrossRef]

20. Catalán, M.; Negrete-Aranda, R.; Martos, Y.M.; Neumann, F.; Santamaría, A.; Fuentes, K. On the intriguing subject of the low amplitudes of magnetic anomalies at the Powell Basin. *Front. Earth Sci.* **2023**, *11*, 1199332. [CrossRef]
21. Martos, Y.M.; Catalán, M. The Drake Passage asthenospheric and oceanic gateway. *Earth-Sci. Rev.* **2024**, *252*, 104731. [CrossRef]
22. Dalziel, I.W.D. The Scotia arc: An international geological laboratory. *Episodes* **1984**, *7*, 7–13. [CrossRef]
23. Maldonado, A.; Balanyá, J.C.; Barnolas, A.; Galindo-Zaldivar, J.; Hernández, J.; Jabaloy, A.; Livermore, R.; Martínez-Martínez, J.M.; Rodríguez-Fernández, J.; De Galdeano, C.S.; et al. Tectonics of an extinct ridge-transform intersection, Drake Passage (Antarctica). *Mar. Geophys. Res.* **2000**, *21*, 43–67. [CrossRef]
24. Eagles, G.; Gohl, K.; Larter, R.D. High-resolution animated tectonic reconstruction of the south Pacific and West Antarctic margin. *Geochem. Geophys. Geosystems* **2004**, *5*, Q07002. [CrossRef]
25. Dalziel, I.W.D. Antarctica and supercontinental evolution: Clues and puzzles. *Earth Environ. Sci. Trans. R. Soc. Edinb.* **2013**, *104*, 3–16. [CrossRef]
26. Maldonado, A.; Bohoyo, F.; Galindo-Zaldívar, J.; Hernandéz-Molina, F.J.; Lobo, F.J.; Lodolo, E.; Martos, Y.M.; Pérez, L.F.; Schreider, A.; Somoza, L. A modelo f oceanic development by ridge jumping opening of the Scotia Sea. *Glob. Planet. Chang.* **2014**, *123*, 152–173. [CrossRef]
27. Eagles, G.; Livermore, R.; Morris, P. Small basins in the Scotia Sea: The Eocene Drake Passage gateway. *Earth Planet. Sci. Lett.* **2006**, *242*, 343–353. [CrossRef]
28. Brown, B.; Gaina, C.; Müller, D. Circum-Antarctic palaeobathymetry: Illustrated examples from Cenozoic to recent times. *Palaeogeogr. Palaeoclimatol. Palaeoecol.* **2006**, *231*, 158–168. [CrossRef]
29. Livermore, R.; Hillenbrand, C.D.; Meredith, M.; Eagles, G. Drake Passage and Cenozoic climate: An open and shut case? *Geochem. Geophys. Geosyst.* **2007**, *8*, Q01005. [CrossRef]
30. Lagabrielle, Y.; Goddeeris, Y.; Donnadieu, Y.; Malavieille, J.; Suarez, M. The tectonic history of Drake Passage and its possible impacts on global climate. *Earth Planet. Sci. Lett.* **2009**, *279*, 197–211. [CrossRef]
31. Bohoyo, F.; Galindo-Zaldívar, J.; Jabaloy, A.; Maldonado, A.; RodríguezFernández, J.; Schreider, A. Extensional deformation and development of deep basins associated with the sinistral transcurrent fault zone of the Scotia-Antarctic plate boundary. *Geol. Soc. Spec. Publ.* **2007**, *290*, 203–217. [CrossRef]
32. King, E.C.; Leitchenkov, G.; Galindo-Zaldivar, J.; Maldonado, A.; Lodolo, E. "Crustal Structure and Sedimentation in Powell Basin". In Geology and Seismic Stratigraphy of the Antarctic Margin, Part 2. *Antarct. Res. Ser.* **1997**, *71*, 75–93.
33. Catalán, M.; Martos, Y.M.; Galindo Zaldivar, J.; Pérez, L.F.; Bohoyo, F. Unveiling Powell Basin's tectonic domains and understanding its abnormal magnetic anomaly signature. Is heat the key? *Front. Earth Sci.* **2020**, *8*, 580675. [CrossRef]
34. Coren, F.; Ceccone, G.; Lodolo, E.; Zanolla, C.; Zitellini, N.; Bonazzi, C. Morphology, seismic structure and tectonic development of the Powell basin, Antarctica. *J. Geol. Soc.* **1997**, *154*, 849–862. [CrossRef]
35. Rodriguez-Fernandez, J.; Balanya, J.C.; Galindo-Zaldivar, J.; Maldonado, A. Tectonic evolution of a restricted ocean basin: The Powell Basin (northeastern antarctic Peninsula). *Geodinámica Acta* **1994**, *10*, 159–174. [CrossRef]
36. Coren, F.; Lodolo, E.; Ceccone, G. Age constraints for the evolution of the northern Powell basin (Antarctica). *Boll. Geofis. Teor. Applicata.* **2000**, *41*, 193–205.
37. Lawver, L.A.; Williams, T.; Sloan, B. Seismic stratigraphy and heat flow of Powell Basin. *Terra Antart.* **1994**, *1*, 309–310.
38. Hernández-Molina, F.J.; Bohoyo, F.; Naveira Garabato, A.; Galindo-Zaldívar, J.; Lobo, F.J.; Maldonado, A.; Rodríguez-Fernández, J.; Somoza, L.; Stow, D.A.V.; Vázquez, J.T. The Scan Basin evolution: Oceanographic consequences of the deep connection between the Weddell and Scotia Seas (Antarctica). In *10th International Symposium on Antarctic Earth Sciences*; SCAR, Ed.; U.S. Geological Survey and The National Academies: Santa Barbara, CA, USA, 2007; Volume EA086, SCAR; pp. 379–407.
39. Hillenbrand, C.D.; Camerlenghi, A.; Cowan, E.A.; Hernández-Molina, F.J.; Lucchi, R.G.; Rebesco, M.; Uenzelmann-Neben, G. The present and past bottom-current flow regime around the sediment drifts on the continental rise west of the Antarctic Peninsula. *Mar. Geol.* **2008**, *255*, 55–63. [CrossRef]
40. Naveira Garabato, A.C.; Heywood, K.J.; Stevens, D.P. Modification and pathways of Southern Ocean Deep Waters in the Scotia Sea. *Deep. Sea Res. Part I Oceanogr. Res. Pap.* **2002**, *49*, 681–705. [CrossRef]
41. Maldonado, A.; Bohoyo, F.; Galindo-Zaldívar, J.; Hernández-Molina, J.; Jabaloy, A.; Lobo, F.J.; Vázquez, J.T. Ocean basins near the Scotia–Antarctic plate boundary: Influence of tectonics and paleoceanography on the Cenozoic deposits. *Mar. Geophys. Res.* **2006**, *27*, 83–107. [CrossRef]
42. Pérez, L.F.; Martos, Y.M.; García, M.; Weber, M.E.; Raymo, M.E.; Williams, T.; Zheng, X. Miocene to present oceanographic variability in the Scotia Sea and Antarctic ice sheets dynamics: Insight from revised seismic-stratigraphy following IODP Expedition 382. *Earth Planet. Sci. Lett.* **2021**, *553*, 116657. [CrossRef]
43. Maldonado, A.; Zitellini, N.; Leitchenkov, G.; Balanyá, J.C.; Coren, F.; Galindo-Zaldıvar, J.; Vinnikovskaya, O. Small ocean basin development along the Scotia–Antarctica plate boundary and in the northern Weddell Sea. *Tectonophysics* **1998**, *296*, 371–402. [CrossRef]
44. Lawver, L.A.; Gahagan, L.M. Evolution of Cenozoic seaways in the circum-Antarctic region. *Palaeogeogr. Palaeoclimatol. Palaeoecol.* **2003**, *198*, 11–37. [CrossRef]
45. Dalziel, I.W.D.; Lawver, L.A.; Pearce, J.A.; Barker, P.F.; Hastie, A.R.; Barfod, D.N.; Davis, M.B. A potential barrier to deep Antarctic circumpolar flow until the late Miocene? *Geology* **2013**, *41*, 947–950. [CrossRef]

46. Barker, P.F.; Lawver, L.A.; Larter, R.D. Heat-flow determinations of basement age in small oceanic basins of the southern central Scotia Sea. *Geol. Soc. Lond. Spec. Publ.* **2013**, *381*, 139–150. [CrossRef]
47. Pérez, L.F.; Lodolo, E.; Maldonado, A.; Hernández-Molina, F.J.; Bohoyo, F.; Galindo-Zaldívar, J.; Burca, M. Tectonic development, sedimentation and paleoceanography of the Scan Basin (southern Scotia Sea, Antarctica). *Glob. Planet. Chang.* **2014**, *123*, 344–358. [CrossRef]
48. Pérez, L.F.; Maldonado, A.; Hernández-Molina, F.J.; Lodolo, E.; Bohoyo, F.; Galindo-Zaldívar, J. Tectonic and oceanographic control of sedimentary patterns in a small oceanic basin: Dove Basin (Scotia Sea, Antarctica). *Basin Res.* **2017**, *29*, 255–276. [CrossRef]
49. Livermore, R.; Eagles, G.; Morris, P.; Maldonado, A. Shackleton Fracture Zone: No barrier to early circumpolar ocean circulation. *Geology* **2004**, *32*, 797–800. [CrossRef]
50. Martos, Y.M.; Maldonado, A.; Lobo, F.J.; Hernández-Molina, F.J.; Pérez, L.F. Tectonics and palaeoceanographic evolution recorded by contourite features in southern Drake Passage (Antarctica). *Mar. Geol.* **2013**, *343*, 76–91. [CrossRef]
51. Quesnel, Y.; Catalán, M.; Ishihara, T. A new global marine magnetic anomaly data set. *J. Geophys. Res.* **2009**, *114*, B04106–B04111. [CrossRef]
52. Lesur, V.; Hamoudi, M.; Choi, Y.; Dyment, J.; Thébault, E. Building the second version of the world digital magnetic anomaly map (WDMAM). *Earth Planets Space* **2016**, *68*, 27. [CrossRef]
53. Alken, P.; Thébault, E.; Beggan, C.D.; Amit, H.; Aubert, J.; Baerenzung, J. International geomagnetic reference field: The thirteenth generation. *Earth Planets Space* **2021**, *73*, 49. [CrossRef]
54. Zhang, Q.; Sun, C.; Yan, F.; Lv, C.; Liu, Y. Leveling airborne geophysical data using a unidirectional variational model. *Geosci. Instrum. Methods Data Syst.* **2022**, *11*, 183–194. [CrossRef]
55. Sandwell, D.T.; Müller, R.D.; Smith, W.H.F.; García, E.; Francis, R. New global marine gravity model from CryoSat-2 and Jason-1 reveals buried tectonic structure. *Science* **2014**, *346*, 65–67. [CrossRef] [PubMed]
56. Becker, J.J.; Sandwell, D.T.; Smith, W.H.F.; Braud, J.; Binder, B.; Depner, J. Global bathymetry and elevation data at 30 arc seconds resolution: SRTM30_PLUS. *Mar. Geod.* **2009**, *32*, 355–371. [CrossRef]
57. Mendel, V.; Munschy, M.; Sauter, D. MODMAG: A MATLAB program to model marine magnetic anomalies. *Comput. Geosci.* **2005**, *31*, 589–597. [CrossRef]
58. Ogg, J.G. *Geomagnetic Time Scales*; Gradstein, F.M., Ogg, J.G., Schmitz, M.D., Ogg, G.M., Eds.; Elsevier: Amsterdam, The Netherlands, 2020; pp. 159–192.
59. Raymond, C.A.; Labrecque, J.L. Magnetization of the oceanic crust-thermoremanent magnetization of chemical remanent magnetization? *J. Geophys. Res.* **1987**, *92*, 8077–8088. [CrossRef]
60. Choe, H.; Dyment, J. Fading magnetic anomalies, thermal structure and earthquakes in the Japan trench. *Geology* **2019**, *48*, 278–282. [CrossRef]
61. Schouten, H.; Tivey, M.A.; Fornari, D.J.; Cochran, J.R. Central anomaly magnetization high: Constraints on the volcanic construction and architecture of seismic layer 2A at a fast-spreading mid-ocean ridge, the EPR at 9°30′–50′N. *Earth Planet Sci. Lett.* **1999**, *169*, 37–50. [CrossRef]
62. Tivey, M.A.; Johnson, H.P. Variations in oceanic crustal structure and implications for the fine-scale magnetic anomaly signal. *Geophys. Res. Lett.* **1993**, *20*, 1879–1882. [CrossRef]
63. Garrett, S.W. Interpretation of reconnaissance gravity and aeromagnetic surveys of the Antarctic Peninsula. *J. Geophys. Res.* **1990**, *95*, 6759–6777. [CrossRef]
64. Barker, P.F. Evolution of the Scotia Sea region: Relevance to broad-band seismology. *Terra Antart.* **2001**, *8*, 67–70.
65. Eagles, G.; Livermore, R.A.; Fairhead, J.D.; Morris, P. Tectonic evolution of the west Scotia Sea. *J. Geophys. Res. Solid Earth* **2005**, *110*, B02401. [CrossRef]
66. Lodolo, E.; Civile, D.; Vuan, A.; Tassone, A.; Geletti, R. The Scotia–Antarctica plate boundary from 35 W to 45 W. *Earth Planet. Sci. Lett.* **2010**, *293*, 200–215. [CrossRef]
67. Barker, P.F.; Barber, P.L.; King, E.C. An early Miocene ridge crest-trench collision on the South Scotia Ridge near 36°W. *Tectonophysics* **1984**, *102*, 315–332. [CrossRef]